Self-Induced Rayleigh-Taylor Instability in Segregating Dry Granular Flows

Umberto D'Ortona*
Aix Marseille Univ., CNRS, Centrale Marseille, M2P2, Marseille, France

Nathalie Thomas
Aix Marseille Univ., CNRS, IUSTI, Marseille, France

(Received 13 November 2019; revised manuscript received 14 February 2020; accepted 1 April 2020; published 29 April 2020)

Dry-granular material flowing on rough inclines can experience a self-induced Rayleigh-Taylor (RT) instability followed by the spontaneous emergence of convection cells. For this to happen, particles are different in size and density; the larger particles are denser but still segregate toward the surface. When the flow is initially made of two layers of particles (dense particles above), a RT instability develops during the flow. When the flow is initially made of one homogeneous layer mixture, the granular segregation leads to the formation of an unstable layer of large, dense particles at the surface, that subsequently destabilizes in a RT plume pattern. The unstable density gradient has been only induced by the motion of the granular matter. This self-induced Rayleigh-Taylor instability and the two-layer RT instability are studied using two different methods: experiments and simulations. At last, contrary to the usual fluid behavior where the RT instability relaxes into two superimposed stable layers of fluid, the granular flow evolves to a pattern of alternated bands corresponding to recirculation cells analogous to Rayleigh-Bénard convection cells where segregation sustains the convective motion.

DOI: 10.1103/PhysRevLett.124.178001

The Rayleigh-Taylor instability is one of the most commonly studied hydrodynamical instabilities. It occurs when a dense fluid is put atop a lighter fluid [1,2]. This phenomenon is encountered in various fields like volcanoes, supernovae explosions, or while pouring vinegar over oil at home. Another frequently studied instability is the Rayleigh-Bénard instability. It occurs when a horizontal layer of fluid is heated from below [3]. The reason for both instabilities is external: the two layers have been superimposed, or heat is brought into the system. But, in this Letter, the granular flow spontaneously creates its unstable state; then, the instability happens, and the flow sustains the convective state without any external cause.

Dry-granular material behaves as liquid when put into motion [4–6]. One striking phenomenon is the granular segregation: when particles of different sizes flow together, large particles migrate to the flow free surface [7–10]. This process results from a grain-scale interaction between large and small particles; it vanishes for a large (respectively, small) particle surrounded only by large (respectively, small) particles. Another segregation occurs when particles having different densities flow together: denser particles migrate to the bottom [11–14]. Depending on size and density ratios, large, dense particles could sink or raise. Here, large, dense particles are chosen such that segregation pushes them toward the surface, creating a reverse unstable density gradient. The system induces its own unstable state simply by flowing, and not because of external causes, which is unusual in fluid mechanics.

To our knowledge, the Rayleigh-Taylor instability between two dry-granular materials of different densities has never been studied, even though several works report Rayleigh-Taylor instabilities involving a granular material and liquid or air [15–17]. This Letter first studies the instability between two initially superimposed dry-granular layers flowing down an incline. Buoyancy acts there as it does in liquids. Second, and more interestingly, a self-induced Rayleigh-Taylor instability may arise when one initially homogeneous mixture layer flows, spontaneously developing an unstable state. The segregation can lead to the formation of a layer of large, dense particles at the surface that will subsequently destabilize through a Rayleigh-Taylor (RT) instability. This new phenomenon involves both an individual behavior of particles through segregation and a collective behavior through a hydrodynamical destabilization of the dense surface layer.

Moreover, when the granular media goes on flowing, a third very surprising phenomenon occurs: both granular flows evolve to a pattern of alternated bands with recirculation cells analogous to Rayleigh-Bénard convection cells. Convection has been observed in rapid granular flows for which the granular temperature plays the role of the temperature in a liquid [18,19]; but, here, a moderate slope is used and flows are dense. The driver of the convection is not the temperature but the segregation, which is induced by the flow itself. The convection is self-sustained by the flow since, during the flow, segregation and buoyancy compete. Our system has similarities with bioconvection

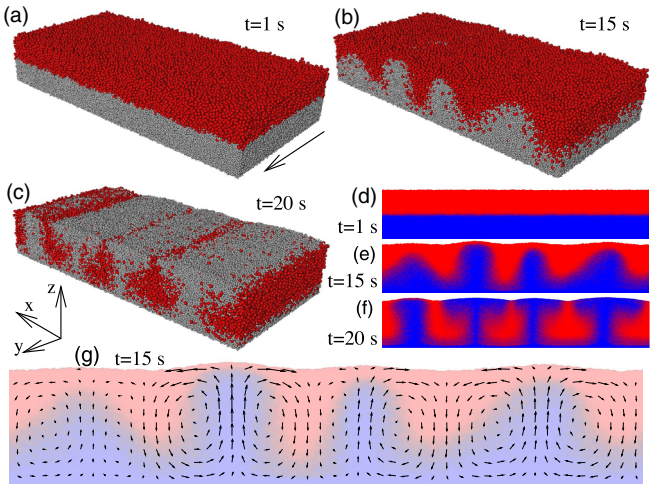

FIG. 1. Rayleigh-Taylor instability in an initially two-layer flow. (a)–(c) Successive pictures of the destabilization (large particles in red). The arrow indicates flow direction. (d)–(f) Concentration fields $(x-z)$ averaged over y. (g) Transverse velocity field $(x-z)$.

induced by upwardly self-propelled denser microorganisms [20], except that our particles are neighbors-propelled instead of self-propelled.

As the three phenomena have never been observed, experiments (below) and numerical simulations using the distinct element method have been conducted. The normal force is modeled using a damped linear spring. The tangential force is of the Cundall and Strack type [21,22]. Small particles have the properties of cellulose acetate: density $\rho = 1308\,\mathrm{kg\,m^{-3}}$, restitution coefficient $e = 0.87$, friction coefficient $\mu = 0.7$, and a diameter $d = 6$ mm. Large particles have the same friction and restitution coefficients, but size d_l and density ρ_l are adjusted, depending on the needs. To prevent crystallization, each species presents a uniform size distribution from $0.95d$ to $1.05d$. The collision time of $\Delta t = 10^{-4}$ s is sufficient for modeling hard spheres [22–25]. Thus, the stiffness and damping coefficients are $k_n = 7.32\,10^4\ \mathrm{N\,m^{-1}}$ and $\gamma_n = 0.206\ \mathrm{kg\,s^{-1}}$ [21,22]. The integration time step is $\Delta t/50 = 2\,10^{-6}$ s for numerical stability [23]. Rough inclines are modeled using a monolayer of bonded small particles randomly placed with a compacity of about 0.57. They have an infinite mass and do not move during the simulation. Flowing particles are randomly placed on the incline, either on a two-layer configuration (large particles above) or in one homogeneous mixture layer configuration. At time zero, gravity is set with an angle of $\theta = 23°$ and the flow starts. Periodic boundary conditions are applied in x and y.

The case of an initially two-layer system, with large, dense particles forming the upper layer, is numerically studied (Fig. 1). The flow thickness is $H = 36d$, the length in the flowing direction is $L = 100d$, and the width is $W = 200d$. The size and density ratios are $d_l/d = 2$ and $\rho_l/\rho = 1.5$ with an equal volume fraction. After the flow start, the interface between the two species destabilizes ($t = 15$ s) and forms a plume pattern ($t = 20$ s) typical of a Rayleigh-Taylor instability obtained with viscous liquids having a viscosity ratio close to one [26] (see Video 1 in the Supplemental Material [27]). As the flow stretches the interface in the y direction, the plumes take the shape of parallel stripes [28]. The plume pattern is visible in concentration fields obtained by averaging the particle volume fraction over y [Figs. 1(d)–1(f)]. Plumes have rising or descending motion through the whole flow thickness with spreading heads at the bottom and surface. The transverse velocity field [Fig. 1(g)] is typical of a RT instability with vertical flow inside the plumes and contrarotative rolls between plumes. The wavelength can be estimated as $\lambda \simeq 1.4H$. Another simulation with $H = 20d$ has given $\lambda \simeq 1.7H$. At the end of the simulation ($t = 70$ s), contrary to the usual RT instability with liquids where the system relaxes into two superimposed layers, the granular flow reaches a pattern of parallel stripes made of pure large particles alternating with stripes made of a mixture of small and large particles [Fig. 2(a)].

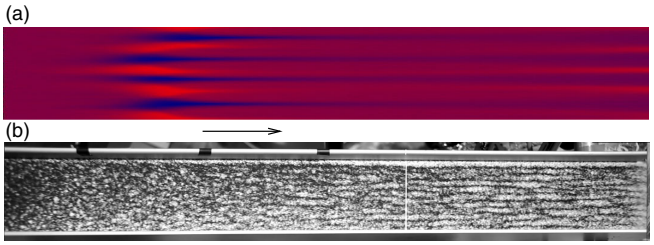

FIG. 2. Rayleigh-Taylor instability in an initially two-layer flow. (a) Space-time diagram viewed from the top; the concentration is averaged over the thickness, and time passes from left to right up to 70 s. (b) Top view of the corresponding experiment. The flow is from left to right (see arrow), and large particles are black. Successive stages of the destabilization are visible from left to right.

Experiments have been conducted on a 110-cm-long 6.85-cm-wide rough incline [Fig. 2(b)]. Flowing particles are ceramic beads: white Zirshot ($d = 250$–$280\ \mu$m, $\rho = 3850\ \mathrm{kg\,m^{-3}}$) and black Cerabeads ($d_l = 500$–$560\ \mu$m, $\rho_l = 6200\ \mathrm{kg\,m^{-3}}$) inducing $d_l/d = 2$ and $\rho_l/\rho = 1.61$. With the chosen thicknesses, W/H is slightly larger in experiments compared to simulations. The channel length, corresponding to the duration time in simulations, is smaller and does not give access to long time evolutions. The incline is first placed horizontally and covered with two superimposed layers of small, light (at bottom) and large, dense particles. It is slowly tilted at 23°, and the gate at the bottom end serves as a containment. At $t = 0$, the gate is removed, and the flow triggering rapidly spreads up the slope. The flow starts everywhere with a small time delay (see Video 2 in the Supplemental Material [27]). Figure 2(b) is taken when the triggering

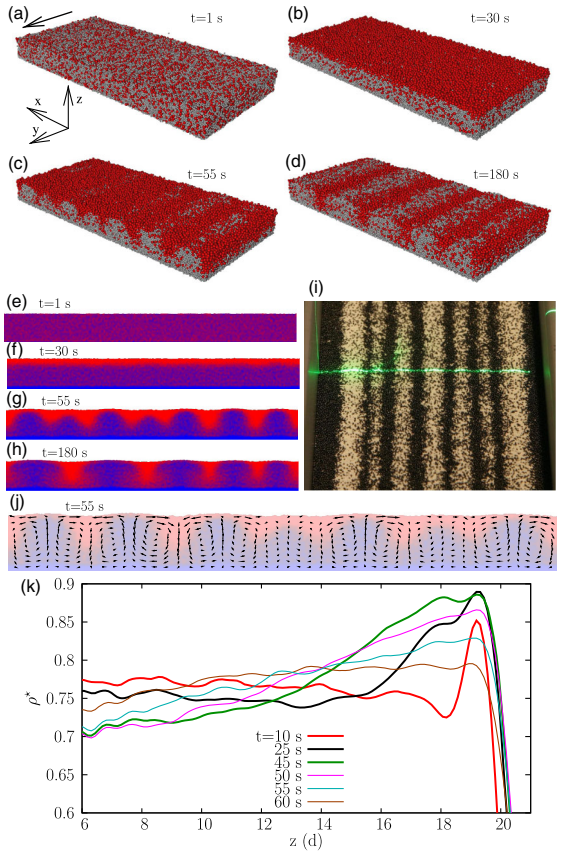

FIG. 3. Self-induced Rayleigh-Taylor instability of one initially homogeneous layer. (a)–(d) Stages of the destabilization. (e)–(h) Concentration fields ($x-z$) averaged over y. (i) Lower part of the experiment. Small variations of flow thickness shown by laser deflection: dark bands (large particles) are depressions. (j) Transverse velocity field. (k) Reduced density profiles near the surface at $z = 20d$.

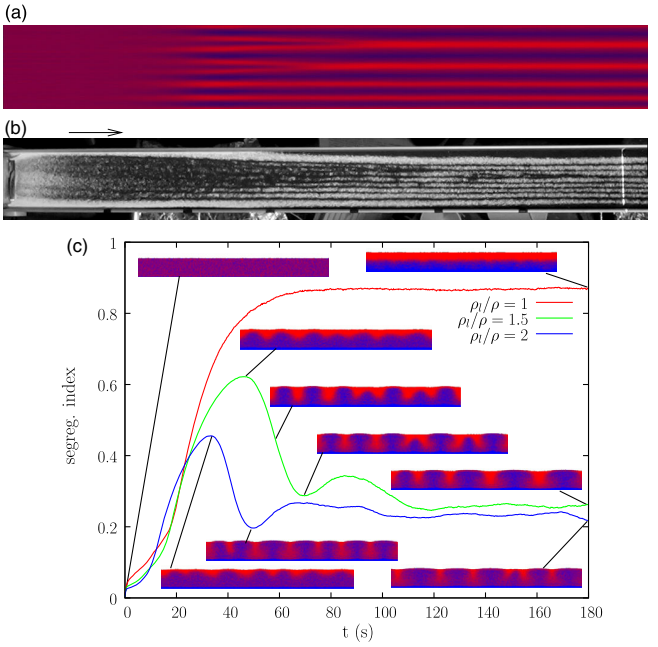

FIG. 4. Self-induced Rayleigh-Taylor instability of an initially homogeneous layer. (a) Space-time diagram of the simulation ($\rho_l/\rho = 1.5$) averaged over z. Time passes horizontally up to 180 s. (b) Experiment ($\rho_l/\rho = 1.61$): a homogeneous mixture is injected at the top (left) of the incline, then segregation appears, and the instability induces the formation of stripes. (c) segregation index (SI) time evolution and corresponding vertical concentration fields. $\rho_l/\rho = 2$ gives similar results, but no instability occurs for $\rho_l/\rho = 1$

reaches the left top of the inclined plane. All successive stages of the Rayleigh-Taylor instability can be seen from left to right: two layers where only the upper layer is visible, with small, white dots showing ascending white particle plumes; and formation of a band pattern. For several experiments, with H from $12d$ to $19d$ (measured with the laser sheet deflection), the wavelength of the pattern is between $1.67H$ and $1.93H$.

The case of an initially homogeneous mixture is now considered numerically and experimentally. In simulations, all physical parameters are identical to Fig. 1, except the flow thickness of $H = 20d$ to reduce computing time (Fig. 3). Between $t = 0$ and $t \simeq 40$ s, the segregation induces the formation of a surface layer of large, dense particles. Then ($40\,\text{s} \lesssim t \lesssim 70$ s), it destabilizes and organizes in stripes parallel to the flow (see Video 3 in the Supplemental Material [27]). The vertical concentration fields [Figs. 3(e)–3(h)] show the formation of the layer of large, dense particles; its destabilization; and the formation of a plume pattern typical of a Rayleigh-Taylor instability.

The transverse velocity field after destabilization is similar to Fig. 1(g). It presents vertical flows aligned with plumes and contrarotative rolls between plumes [Fig. 3(j)]. Both plumes and rolls spread on the whole thickness. The free surface is not flat, stripes of large particles correspond to hollows, and stripes of the mixture are bumpy [Fig. 3(h)]. This phenomenon is observed experimentally using a laser sheet deflection [Fig. 3(i)]. Dark bands correspond to depressions around 0.1 mm deep. Rayleigh-Taylor instabilities are associated with an unstable density gradient. The reduced density $\rho^\star$, which is the bulk density divided by ρ, is equal to 0.59 for small particles (random loose packing [29]); to 0.88 for large, dense particles; and to 0.78 for a 50% volume mixture. Reduced density profiles show the accumulation of one-to-two pure layers of large beads at the surface, an increased concentration of these beads near the surface, and the formation of an unstable density gradient [Fig. 3(k)]. The maximal gradient takes place from $\rho^\star = 0.88$ to 0.75 on around $8d$ thick. Destabilization starts (between 45 and 50 s), and the gradient rapidly vanishes when plumes cross over.

Experimentally, for the initially homogeneous flow [Fig. 4(b)], the incline is initially empty and a feeding container is added at the top (not seen), reducing the incline to 91 cm. It is filled with about 400 alternated thin layers of

small and large particles to provide a feeding as homogeneous as possible. At $t = 0$, the container gate is opened and the flow starts. Figure 4(b) is taken in the stationary regime.

All stages of the instability are visible: the granular flow is initially homogeneous ($0 \lesssim x \lesssim 10$ cm), granular segregation drives large particles to the surface (10 cm$\lesssim x \lesssim 20$ cm), destabilization occurs (20 cm$\lesssim x \lesssim 40$ cm), and the flow organizes in a pattern of parallel stripes ($x \gtrsim 40$ cm) (see Video 4 in the Supplemental Material [27]). Quantitatively, the experiment length $L \simeq 3400d$ corresponds to the simulation flowing time $t \simeq 60$ s, i.e., one-third of the space-time diagram [Fig. 4(a)]. Several experiments give wavelengths for the initial destabilization from $\lambda \simeq 1.75H$ to $1.93H$. The flow thicknesses are from $H = 9d$ to $16d$. The spreading of the experimental measurements is due to thickness irregularities but is nevertheless in good agreement with the simulation wavelength $\lambda \simeq 40d \simeq 2H$.

The evolution of the segregation is quantified using a segregation index:

$$\mathrm{SI} = 2\frac{CM_l - CM}{H}, \tag{1}$$

with CM_l and CM as the vertical positions of the mass center for large and small particles, respectively. The SI varies from 1 (perfectly segregated: large particles above) to -1 (reversed segregation: small particles above); and 0 corresponds to a homogeneous layer. For the density ratio $\rho_l/\rho = 1.5$, the SI increases up to 0.6 ($t \simeq 45$ s) and subsequently decreases while the system destabilizes to reach a stationary value [Fig. 4(c)]. For $\rho_l/\rho = 2$, the destabilization occurs more rapidly following the same overall phenomenon. No instability occurs for $\rho_l/\rho = 1$ because no density gradient counterbalances the upward segregation. Simulations for $\rho_l/\rho = 1$ have been performed up to 400 s; initially, homogeneous and two-layer cases both evolve toward a stable interface between two layers (large particles above). Experimentally, in a channel, particle mixtures ($\rho_l/\rho = 1$; $d_l/d = 1.75$, 2, and 3.5) evolve toward a uniform stable layer of large particles on the pure bottom layer of small particles [8]. Both systems with $\rho_l/\rho = 1$ remain stable with no axial banding, in agreement with a RT instability mechanism.

Our numerical and experimental results are valid in a range of slope angles (numerically from 22 to 26°): material flows and segregation happens (no collisional regime). For a larger angle, destabilization happens earlier but further down because the flow is faster.

The instability numerically happens for the density ratio as low as 1.2 (for $d_l/d = 2$). The question of a threshold is still under investigation. There is no surface tension as in liquids. Nevertheless, other stabilizing mechanisms may occur as the high random particle motion of granular flows.

Self-induced RT instability could appear paradoxical, but it results from the competition between segregation and buoyancy, with variable intensities. We choose the size and density ratios such that, in the mixture, the segregation is dominant over the individual particle buoyancy. Large particles move upward while surrounded by the mixture and accumulate at the surface in a layer where there is no small particle. In this layer, buoyancy acts in a collective hydrodynamical process because dense particles are close enough, buoyancy dominates, and the whole surface layer develops a RT instability.

A band pattern also appears in partially filled rotating drums experiencing axial segregation [30–41]. The mechanism, still under debate [37], is likely due to a free surface slope difference between species [32,33]. But, there is no slope difference in RT instability on inclines, even though there are some undulations. Slope differences between bands are null in simulations (periodic boundaries) and could not exceed $1/100°$ in experiments. Moreover, in cylinders, axial segregation can happen even for $\rho_l/\rho = 1$ [30,31], contrary to RT instability on incline [Fig. 4(c)]. Furthermore, in drums, large particle bands form above a core of small particles [37,39]. In RT instability, sinking and raising plumes present an almost symmetrical pattern, intersecting vertically the whole thickness. The raising bands are composed of a mixture, contrary to the pure small particle bands in drums [32,39,40]. Finally, the RT instability is more rapid to occur, only flowing over around $2000d$ induces the instability. In drums, bands appear after at least several hundred revolutions, and often after few thousand revolutions [32,35,41]. The self-induced RT instability and axial segregation in tumblers are different mechanisms.

At last, the long time evolution of the instability is considered up to $t = 250$ s. The thickness of the flow is $H = 24d$, $\rho_l/\rho = 2$, and the flow length is reduced to $L = 30d$. Both the two-layer system, through a usual Rayleigh-Taylor instability, and the homogeneous mixture, through a self-induced Rayleigh-Taylor instability, converge toward the same SI value and parallel stripe patterns (Fig. 5). The space-time diagrams show bands merging associated to a slight SI decrease (arrows). They both converge toward the same stationary regime, whose wavelength is larger than those of the initial destabilization. Similar behaviors with persisting bands and bands merging have been observed in experiments for low thicknesses. The series of contrarotative rolls are sustained, corresponding to the positions of concentration plumes [Fig. 5(d)–5(e)]. The figures are analogous to Rayleigh-Bénard convection cells [3]. The maximal transverse velocity reaches 2% of the mean velocity in the flowing direction. The driver of this convection is the granular segregation that lifts large particles to the surface even though they are denser. As buoyancy drives denser regions downward and segregation drives large, dense particles upward, the cells are sustained.

Size segregation is both the cause for the self-induced Rayleigh-Taylor instability and for the self-sustained

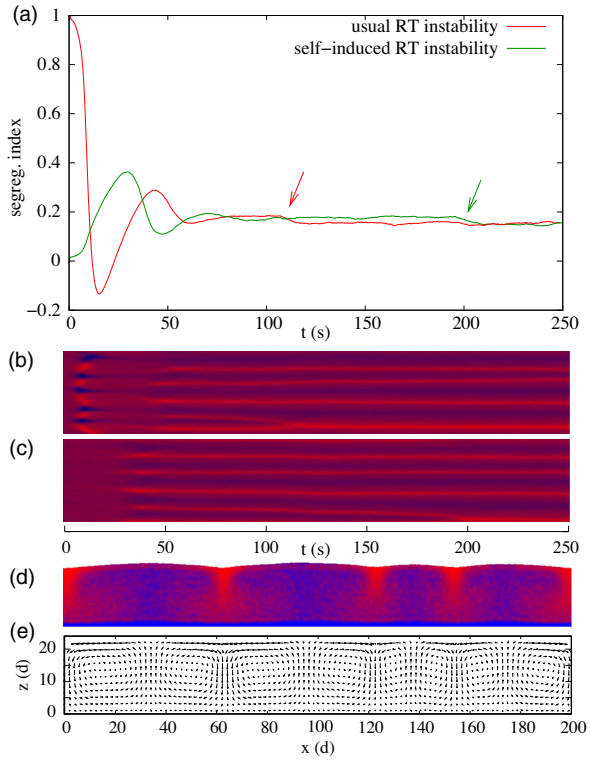

FIG. 5. Stationary regime. (a) Time evolution of the segregation index for both initial conditions: two-layer and homogeneous cases. Arrows indicate band merging. Space-time diagrams for an initially (b) two-layer or (c) homogeneous flow. (d) Volume concentration field and (e) corresponding velocity map $(x - z)$ of the initially homogeneous flow averaged on the last 40 s.

Rayleigh-Bénard convection. By flowing, the homogeneous layer creates its own unstable state, which is quite unusual, but is not able to maintain the dense layer at the surface: the system evolves to a self-sustained convective state. Nevertheless, this very simple system (flowing particles having different sizes and densities) brings the sufficient mechanisms to induce self-organization, pattern formation, and instability, which are features usually met in complex systems like biological systems [20] or complex chemical reactions [42]. In a strange way, the granular segregation creates an automixing system with large scale heterogeneities, instead of a separating process.

We thank S. Gsell and N. Fraysse for interesting comments. Centre de Calcul Intensif d'Aix-Marseille University is acknowledged for granting access to its high performance computing resources.

*umberto.d-ortona@univ-amu.fr

[1] S. Chandrasekhar, *Hydrodynamic and Hydromagnetic Stability* (Dover, New York, 1981).
[2] F. Charu, *Hydrodynamic Instabilities* (Cambridge University Press, Cambridge, England, 2011).
[3] A. V. Getling, *Rayleigh-Bénard Convection: Structures and Dynamics* (World Scientific, Singapore, 1998).
[4] J. Duran, *Sands, Powders, and Grains: An Introduction to the Physics of Granular Materials* (Springer-Verlag, New York, 2000).
[5] H. J. Herrmann, J.-P. Hovi, and S. Luding, *Physics of Dry Granular Media* (Springer, Dordrecht, Netherlands, 1998).
[6] B. Andreotti, Y. Forterre, and O. Pouliquen, *Granular Media: Between Fluid and Solid* (Cambridge University Press, Cambridge, England, 2013).
[7] M. E. Möbius, B. E. Lauderdale, S. R. Nagel, and H. M. Jaeger, Nature (London) **414**, 270 (2001).
[8] N. Thomas, Phys. Rev. E **62**, 961 (2000).
[9] T. Shinbrot, Nature (London) **429**, 352 (2004).
[10] N. Thomas and U. D'Ortona, Phys. Rev. E **97**, 022903 (2018).
[11] J. M. Ottino and D. V. Khakhar, Annu. Rev. Fluid Mech. **32**, 55 (2000).
[12] G. Félix and N. Thomas, Phys. Rev. E **70**, 051307 (2004).
[13] N. Jain, J. M. Ottino, and R. M. Lueptow, Granular Matter **7**, 69 (2005).
[14] A. Tripathi and D. V. Khakhar, J. Fluid Mech. **717**, 643 (2013).
[15] C. Völtz, W. Pesch, and I. Rehberg, Phys. Rev. E **65**, 011404 (2001).
[16] I. C. Carpen and J. F. Brady, J. Fluid Mech. **472**, 201 (2002).
[17] J. L. Vinningland, Ø. Johnsen, E. G. Flekkoy, R. Toussaint, and K. J. Måløy, Phys. Rev. Lett. **99**, 048001 (2007).
[18] Y. Forterre and O. Pouliquen, Phys. Rev. Lett. **86**, 5886 (2001).
[19] T. Börzsönyi, R. E. Ecke, and J. N. McElwaine, Phys. Rev. Lett. **103**, 178302 (2009).
[20] N. A. Hill and T. J. Pedley, Fluid Dyn. Res. **37**, 1 (2005).
[21] J. Schäfer, S. Dippel, and D. E. Wolf, J. Phys. I (France) **6**, 5 (1996).
[22] U. D'Ortona, N. Thomas, and R. M. Lueptow, Phys. Rev. E **93**, 022906 (2016).
[23] G. H. Ristow, *Pattern Formation in Granular Materials* (Springer-Verlag, Berlin, 2000).
[24] C. S. Campbell, J. Fluid Mech. **465**, 261 (2002).
[25] L. E. Silbert, G. S. Grest, R. Brewster, and A. J. Levine, Phys. Rev. Lett. **99**, 068002 (2007).
[26] W. D. Woidt, Tectonophysics **50**, 369 (1978).
[27] See Supplemental Material at http://link.aps.org/supplemental/10.1103/PhysRevLett.124.178001. Video 1: Numerical RT instability of an initially bi-layer flow. Video 2: Experimental RT instability of an initially bi-layer flow. Video 3: Numerical RT instability of an initially homogeneous mixture. Video 4: Experimental RT instability of an initially homogeneous mixture.
[28] C. H. Yu, M. Y. Chang, and T. F. Lin, Int. J. Heat Mass Transfer **40**, 333 (1997).
[29] F. A. L. Dullien, *Porous Media: Fluid Transport and Pore Structure*, 2nd ed. (Academic Press, San Diego, 1992).
[30] R. Khosropour, E. Valachovic, and B. Lincoln, Phys. Rev. E **62**, 807 (2000).
[31] T. Finger, A. Voigt, J. Stadler, H. G. Niessen, L. Naji, and R. Stannarius, Phys. Rev. E **74**, 031312 (2006).
[32] K. M. Hill and J. Kakalios, Phys. Rev. E **49**, R3610 (1994).

[33] H. Caps, R. Michel, N. Lecocq, and N. Vandewalle, Physica (Amsterdam) **326A**, 313 (2003).
[34] S. J. Fiedor and J. M. Ottino, Phys. Rev. Lett. **91**, 244301 (2003).
[35] A.-N. Huang, L.-C. Liu, and H.-P. Kuo, Powder Technol. **239**, 98 (2013).
[36] A. C. Santomaso, R. Artoni, and P. Canu, Chem. Eng. Sci. **90**, 151 (2013).
[37] P. Chen, J. M. Ottino, and R. M. Lueptow, New J. Phys. **13**, 055021 (2011).
[38] M. Newey, J. Ozik, S. M. van der Meer, E. Ott, and W. Losert, Europhys. Lett. **66**, 205 (2004).
[39] N. Taberlet, M. Newey, P. Richard, and W. Losert, J. Stat. Mech. (2006) P07013.
[40] T. Finger, M. Schröter, and R. Stannarius, New J. Phys. **17**, 093023 (2015).
[41] K. Choo, M. W. Baker, T. C. A. Molteno, and S. W. Morris, Phys. Rev. E **58**, 6115 (1998).
[42] A. A. Golovin, B. J. Matkowsky, and V. A. Volpert, SIAM J. Appl. Math. **69**, 251 (2008).